New functions of VCSEL-based optical devices

Invited Paper

Fumio Koyama

Microsystem Research Center, Precision and Intelligence Laboratory, Tokyo Institute of Technology
4259-R2-22 Nagatsuta, Midori-ku, Yokohama 226-8503, Japan

Received August 5, 2008

We have seen a lot of unique features off vertical cavity surface emitting lasers (VCSELs), such as low power consumption, wafer-level testing, small packaging capability, and so on. The market of VCSELs has been growing up rapidly in recent years and they are now the key devices in local area networks using multi-mode optical fibers. In addition, new functions on VCSELs have been demonstrated. In this paper, the recent advances of VCSEL photonics will be reviewed, which include the wavelength engineering and the athermal operation based on microelectro mechanical system (MEMS) technologies. Also, this paper explores the potential and challenges for new functions of VCSELs, including high-speed control of optical phase, slow light devices, plasmonic VCSELs, and so on.

OCIS codes: 140.0140, 230.0230, 250.0250, 130.0130.
doi: 10.3788/COL20080610.0755.

1. Introduction

Metro or local area networks have seen great capacity demand. Optical interconnections among network equipments are also becoming important. For these short-reach applications, important issues for light sources are small size and low cost. A vertical cavity surface emitting laser (VCSEL) has been developed since 1977[1]. We have seen various applications including datacom, sensors, optical interconnects, spectroscopy, optical storages, printers, laser displays, laser radar, atomic clock, optical signal processing, and so on. A lot of unique features have been shown, like low power consumption, a wafer level testing, and so on. The market of VCSELs has been growing up rapidly and they are now the key devices in local area networks based on multi-mode optical fibers. Also, long wavelength VCSELs are currently attracting much interest in single-mode fiber metropolitan area and wide area networks[2−12].

In this paper, our recent research activities on VCSEL photonics will be reviewed. We present the wavelength engineering of VCSEL arrays used in high speed short-reach systems, which includes the wavelength integration and wavelength control. The joint research project on ultra-parallel optical links based on VCSEL technologies will be introduced for high speed local-area-networks (LANs) of 100 Gbps or higher. The small footprint of VCSELs allows us to form a densely packed VCSEL array both in space and in wavelength. The wavelength engineering of VCSELs may open up the ultra-high capacity networking. Highly controlled multi-wavelength VCSEL array and novel multi-wavelength combiners are developed toward Tera-bit/s-class ultrahigh capacity parallel optical links.

In addition, the microelectro mechanical system (MEMS)-based VCSEL technology enables widely tunable operations[13]. The recent activity with nano-mechanical tuning scheme with high contrast grating results in the increase of tuning speed[14]. Also we proposed and demonstrated a "athermal VCSEL" with avoiding temperature controllers for uncooled wavelength division multiplexing (WDM) applications[15,16]. The temperature dependence of long-wavelength VCSELs could be reduced by a factor of 50 with a novel thermally-actuated membrane mirror.

In addition, new functions on VCSELs for optical signal processing are addressed. We present an optical nonlinear phase shifter based on a VCSEL saturable absorber[17]. A large nonlinear phase shift can be observed in both modeling and experiments. The proposed device will be useful for mitigating fiber nonlinearities in optical domain and for optically manipulating the phase of light.

Also, highly reflective periodic mirrors commonly used in VCSELs enables us to manipulate the speed of light. This new scheme provides us ultra-compact intensity modulators, optical switches, and so on for VCSEL-based photonic integration. We present our results on the modeling and experiments of VCSEL-based slow light devices.

2. Wavelength engineering and athermalization

The on-wafer wavelength control can be realized by grading the epitaxial layer thickness of a single-mode VCSEL structure. Two-dimensional multiple-wavelength VCSEL arrays were first realized by using an inherent beam flux gradient in multi-band excitation (MBE) growth[18]. When we use metal-organic chemical vapor deposition (MOCVD) on a patterned substrate, the local gradient of the chemical species in the gas phase changes the growth rate. The first MOCVD grown multi-wavelength VCSEL array was demonstrated based on this technique[19]. Several reports on multiple-wavelength VCSELs emitting at 850 and 980 nm have been presented[20−22].

The schematic structure of a 1.2 μm GaInAs/GaAs VCSEL for multi-wavelength VCSEL arrays is shown in Fig. 1. We realized the wavelength extension of GaInAs/GaAs strained quantum wells to open up a new wavelength band of $1.0 - 1.2$ μm[23,24]. We achieved a low-threshold current of below 1 mA, high-temperature operation of up to 450 K, uncooled 10-Gbps operations, and high reliability more than 2000 h[25]. The device

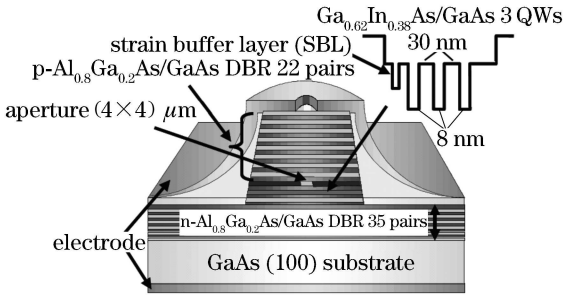

Fig. 1. Schematic structure of GaInAs/GaAs VCSEL[25].

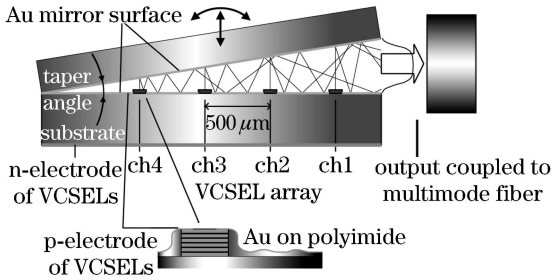

Fig. 3. Schematic structure of a tapered hollow waveguide multiplexer for multi-wavelength VCSEL array[29].

shows a single-mode output power over 2 mW. A characteristic temperature T_0 is over 200 K, which is much higher than 1.3-μm InP based lasers. The excellent temperature characteristic is due to the deep potential well of this material system. The extension of the emission wavelength up to 1.2 μm enables high speed data transmission in single mode fibers. The optical feedback sensitivity is an important issue for low cost single-mode laser diode (LD) module[25]. The increase of the relaxation oscillation frequency enables isolator-free single-mode fiber transmission[25,26].

For upgrading bit rates beyond several tens Gbps, we may expect the use of WDM links even for short reach systems. For this purpose, a multiple-wavelength VCSEL array will be a key device. We have spent much effort on realizing multiple-wavelength VCSEL array on patterned substrates[27]. We demonstrated a single-mode multiple-wavelength VCSEL array on a patterned GaAs substrate as shown in Fig. 1. By optimizing a pattern shape, we achieved multiple-wavelength operation with widely and precisely controlled lasing wavelengths. The maximum lasing span reaches 190 nm[27]. We also demonstrated a densely integrated multi-wavelength VCSEL array of 110 channel with separation of 0.1 nm by thermal tuning scheme as shown in Fig. 2[28].

In order to realize WDM transceivers based on multi-wavelength VCSEL arrays, however, a low-cost and compact multiplexer of each VCSEL output is necessary. We proposed a tapered hollow waveguide multiplexer for coupling multi-wavelength VCSEL array output into a multi-mode fiber as shown in Fig. 3[29]. The structure consists of two high-reflectivity mirrors. The core is air and a VCSEL array is integrated on the bottom mirror in the figure. Each output from VCSEL is radiated vertically from the bottom mirror side. An upper mirror and bottom mirror are placed with a taper angle. After multiple reflections, the reflection angle of the output is simply changed. Therefore the propagation direction of the output from each VCSEL is converted to a horizontal direction. The output from the tapered hollow waveguide multiplexer can be coupled to a multimode fiber and simple and low-cost multiplexer can be realized without losing the advantages of small footprint of VCSEL arrays. We demonstrated multiplexing of 4-channel output of a VCSEL array formed on a patterned substrate for coupling into a multi-mode fiber. The proposed hollow waveguide multiplexer is helpful for realizing compact, simple, and low-cost WDM transceiver for short reach applications.

The temperature dependence of semiconductor lasers, which is typically 0.1 nm/K even for single-mode semiconductor lasers, is a remaining problem. The elimination of costly thermoelectric controllers is desirable for the use in low-cost WDM networks. If it is realized, we expect low power consumption as well as small packaging. We proposed an athermal VCSEL with a fixed wavelength even under temperature changes using the self-compensation based on a thermally actuated cantilever structure[15]. We have demonstrated small temperature dependence in micromachined vertical cavity optical filters and light emitters of GaAs/GaAlAs materials[30]. It is a challenge to realize an athermal VCSEL based on the proposed concept.

Figure 4 shows the schematic structure of a micromachined VCSEL. The base structure of the devices was grown in Corning Incorporated, which is similar to that of InP-based VCSELs with tunnel junction[12]. Because GaInAsP has a larger thermal expansion coefficient than InP, we are able to obtain the thermal actuation of the cantilever for compensating the temperature dependence of wavelength.

The scanning electron microscope (SEM) view of a micromachined InP-based VCSEL is shown in Fig. 5[16]. The cantilever length is varied from 65 to 95 μm, which

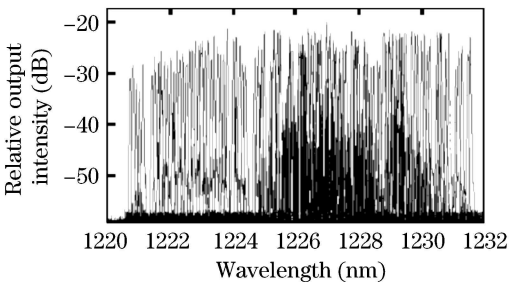

Fig. 2. Lasing spectra of 110 channel VCSEL array[28].

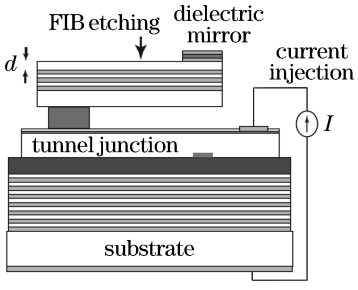

Fig. 4. Schematic of athermal VCSEL[16].

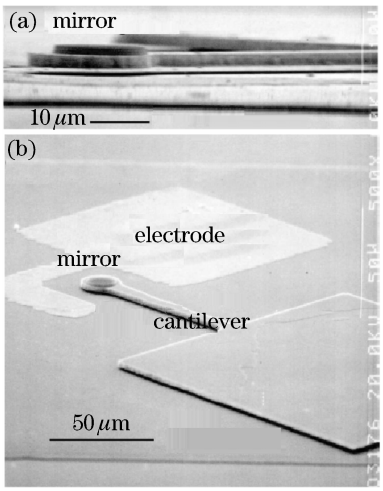

Fig. 5. SEM image of athermal InP-based VCSEL with a thermally-actuated cantilever structure[16].

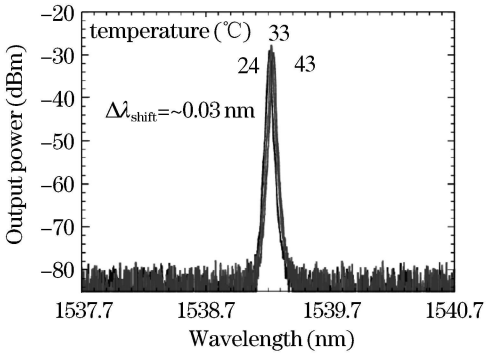

Fig. 6. Athermal operation with a fixed bias current of 4 mA[16].

give us different temperature dependences. The threshold is 1.3 mA and the maximum power is 0.3 mW under room temperature continuous-wave (CW) operation. The device was operated at a constant current of 4 mA to avoid the effect of self-heating. The measured lasing spectra of VCSELs are shown in Fig. 6 for cantilever length of 95 μm. The lowest temperature dependence we achieved is as low as 0.0016 nm/K[16], which is 50 times smaller than that of conventional single mode lasers.

3. Injection licking for optical signal processing

In contrast to the optoelectronic regenerators, all-optical regenerators have a potential for low power consumption, as well as simple and cost-effective configuration. All-optical signal processing using VCSELs has recently been investigated for future photonic networks. The optical injection locking is very useful for reducing chirp and for extending the modulation bandwidth[31]. We are also able to obtain a nonlinear transfer function which can be used for all-optical signal processing. The injection locking of VCSELs has been examined theoretically and experimentally[32−34]. It was shown that a variety of interesting nonlinear behaviors were observed, which were dependent on injection power and frequency detuning. All-optical format conversion was demonstrated using a polarization switching in a VCSEL[35]. All-optical inverter based on transverse mode switching in a two-mode VCSEL was proposed, which has attractive features of low power consumption, dense packaging, and polarization insensitivity[36]. The transverse mode switching is induced when a first-high-order mode was injection-locked by a signal light. The dominant lasing mode switches from a fundamental mode to the high-order mode due to injection locking. If we look at the output power of the fundamental mode as a function of the input power, an optical inverter function with abrupt switching is obtained.

An external light from a tunable laser diode was injected through a standard single mode fiber into a 1.55-μm InP-based VCSEL with a 7-μm circular tunnel junction aperture, which was fabricated in Corning Incorporated[12]. The dominant lasing mode at the bias current was the fundamental mode. When a high-order mode is injection-locked, an optical inverter function was obtained as shown in Fig. 7. An abrupt modal switching with a large extinction ratio more than 25 dB was obtained. The difference in threshold input power between the two orthogonal polarization inputs was as low as $\sim$ 13%. The proposed inverter operated even for the input signal with random polarization, showing a possibility of polarization insensitive operation. The obtained step-like transfer function would be useful for optical regeneration. A distorted signal of 1 Gbps nonreturn-to-zero (NRZ) pseudo-random bit sequence with a word length of $2^7 - 1$ bit is injected into the VCSEL. Figure 8 shows eye diagrams of (a) the input signal and (b) the regenerated signal. The distorted input signal is successfully regenerated. The measured back-to-back bit error ratio (BER) before and after regeneration shows a receiver-sensitivity improvement of 1.2 dB at BER of 10^{-9} after the optical regeneration. The output waveform has been degraded by the relaxation oscillation of the VCSEL. Therefore, the switching speed of the VCSEL-based inverter is partly limited by the

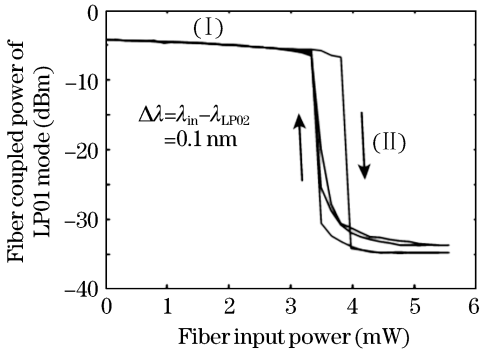

Fig. 7. Optical input/output characteristics of the VCSEL with external light injected into the LP02 mode. The polarizations of the input light are (I) parallel and (II) orthogonal to that of the dominant lasing mode[36].

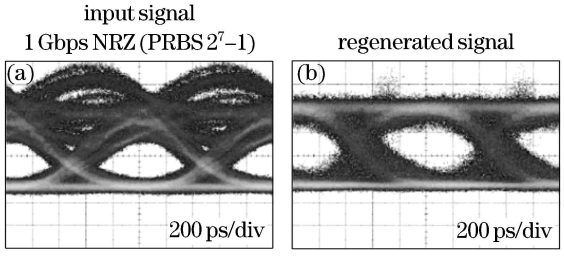

Fig. 8. Eye diagrams of NRZ data at 1 Gbps. (a) Input signal and (b) regenerated signal[36].

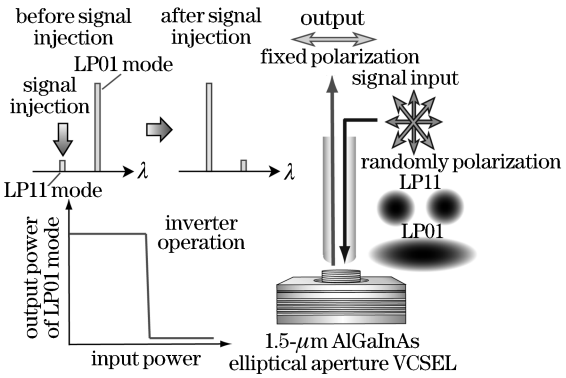

Fig. 9. All-optical polarization control using an injection locked VCSEL input signal[37].

modulation bandwidth of the VCSEL. It could be improved to be beyond 10 Gbps by using a VCSEL with over a 10-Gbps modulation bandwidth, which was already demonstrated[26]. The VCSEL structure may provide us possibilities of low power consumption and polarization insensitive operations for all-optical signal processing.

The polarization control of randomly polarized signal light in single-mode fibers is one of the remaining issues for future photonic networks with polarization- dependent optical devices. All-optical polarization control is a challenging subject for high speed polarization control. The elliptical-shaped VCSEL cavity enables us to obtain stable polarization for a fundamental transverse mode, while two orthogonal polarization states of the high-order transverse mode are degenerate. Figure 9 shows the operating principle of an all-optical polarization controller using an elliptical-apertured VCSEL. When input light is injected to the high-order mode of a VCSEL, the dominant lasing mode is abruptly switched from the fundamental mode to the high-order mode due to injection locking. Thus, the output of the fundamental mode shows an inverter behavior as a function of the input light into the high-order mode. The numerical simulation shows that two orthogonal polarization states of LP11 high order modes are degenerate while the polarization state of the LP01 fundamental transverse mode can be fixed for a properly designed elliptical-shaped VCSEL. When we inject signal light into the high-order mode, the switching characteristics of the LP11 high-order modes can be polarization-insensitive. On the other hand, the polarization state of the fundamental mode can be fixed with the help of an elliptical shape. Thus, the input signal of randomly polarized light can be converted to the output of the fundamental mode with a fixed linear polarization state. The modulation waveform can be transferred to the output of the fundamental mode with signal inversion.

A 1.52-μm VCSEL with a 5×10 (μm) elliptical-shaped tunnel junction aperture was fabricated[37]. The VCSEL structure is the same as that in Ref. [12] except for the shape of the tunnel junction aperture. The threshold current is 1.4 mA. A CW light from a tunable laser is injected into the high-order mode of the VCSEL through a lensed single-mode fiber. The output of the fundamental-mode is coupled to the same fiber and is detected through an optical circulator and a polarizer.

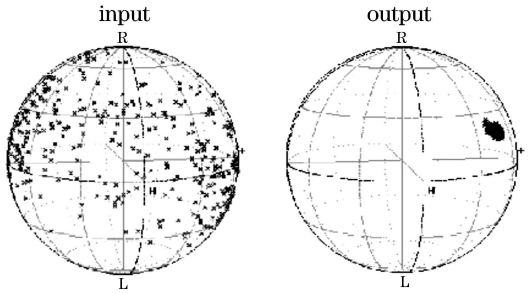

Fig. 10. All optical polarization control of VCSEL-based polarization controller: Polarization states with Poincare spheres[37].

The polarization state of the fundamental mode could be controlled along the major axis of the elliptical tunnel junction. The input light with an input power of 10 mW in the fiber were injected along two orthogonal polarizations, showing polarization- insensitive transverse mode switching. When the polarization of the input light was scrambled by using a polarization scrambler as shown in Fig. 10, large intensity fluctuations through a polarizer were seen. On the other hand, polarization fluctuations of output could be perfectly suppressed with signal inversion, resulting in all-optical polarization control can be realized as shown in Fig. 10. The proposed structure based on an injection-locked VCSEL may enable high-speed optical polarization control for use in future photonic networks.

4. Manipulation of optical phase

Fiber nonlinearities are dominant limiting factors for high-speed transmission systems of 40 Gb/s or beyond. Waveform distortion is induced by various fiber nonlinear effects such as self-phase modulation (SPM), cross-phase modulation (XPM), and four-wave mixing (FWM). The fiber nonlinear effects cannot be compensated by linear optical circuits in optical domain. If we realize a nonlinear optical compensator, which gives us a negative phase-shift in an opposite sign of optical Kerr effect in fibers, we are able to compensate fiber nonlinealities by inserting the device. An optical nonlinear phase-shifter based on a VCSEL structure with a saturable absorber was demonstrated[38].

Figure 11 shows the schematic structure and the operating principle of the optical phase shifter based on the 1.55-μm VCSEL structure[17]. An intensity dependent negative refractive index change appears with an opposite sign of optical Kerr effect in the saturable absorber, which is enhanced by a resonant vertical-cavity. The modeling result shows that either positive or negative phase-shifts of reflected light can be obtained with 1.55 μm-VCSEL, depending on the cavity Q-value[38]. Both positive and negative phase shifts are useful for the compensation of laser chirp and fiber nonlinearities in optical domain, respectively.

There is the trade-off between the phase-shift and optical bandwidth. Therefore, we have to choose suitable design of mirrors for optimizing bandwidth and phase-shift. An InGaAlAs saturable absorber is sandwiched by the two mirrors. If the input light power coupled to this device increases, the phase difference is induced by the refractive index change in the saturable absorber.

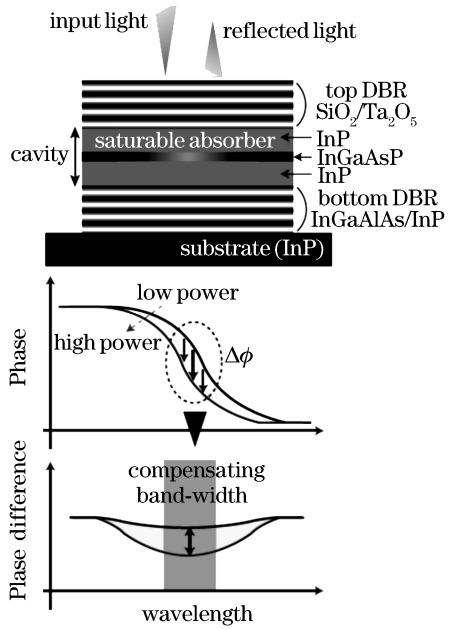

Fig. 11. Schematic structure and operating principle of nonlinear-effect optical compensator using InGaAlAs vertical cavity saturable absorber[23].

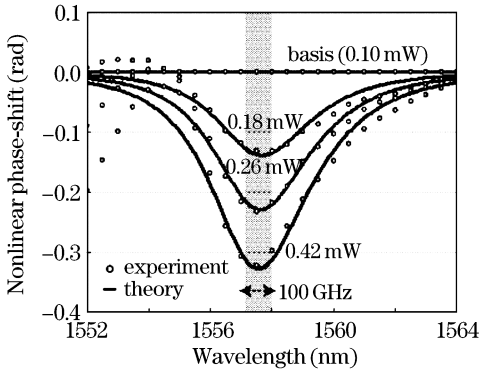

Fig. 12. Measured wavelength dependence of nonlinear phase shift for different input power[38].

No reverse bias gives slow recovery time of 1-ns range. The reflectivity and the group delay dependence on the input power was measured by using an optical component analyzer (Advantest Q7761) with a tunable laser source. The phase shift was estimated from performing spectral domain integration of the measured group delay. Figure 12 shows the nonlinear phase-shift from the data of 0.10 mW input power. The solid lines show the calculation[38]. Here, we assume that saturation coefficient is 2 kW/cm^2, which corresponds to the case of τ=1ns recovery time for a saturable absorber without reverse bias. A positive group delay and negative phase-shifts were observed as predicted in theory. We obtained a large negative phase-shift of a -0.4 radian for the input power of 0.42 mW, which is large enough for compensating 100 km long fiber nonlinearities. The reduction of absorption recovery time below 10 ps with reverse bias enables us to use the compensator for high bit-rate signals. The addition of 1.2 V reverse-bias showed the transient response of nonlinear phase shifts even for 7 ps input pulses.

We carried out the optical compensation of self-phase

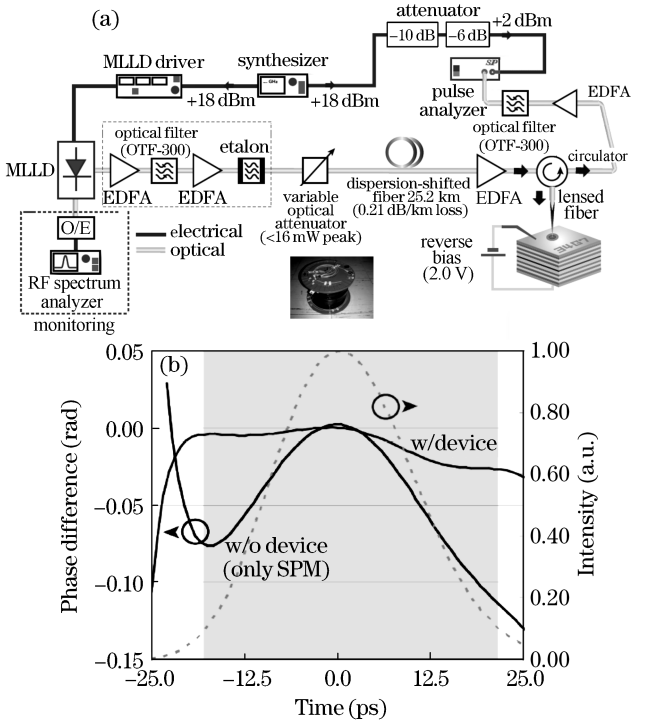

Fig. 13. (a) Measurement setup for all optical compensation of fiber nonlinearity and (b) measured nonlinear-phase shift[39].

modulation for high-speed signals by using our VCSEL-based compensator as shown in Fig. 13(a)[39]. As can be seen in Fig. 13(b), the transient phase change induced by SPM with an input peak power of 8 mW can be optically compensated by using our VCSEL-based compensator. The tail of residual phase-shift (imperfect compensation) would be due to the insufficnt recovery time of photo-carries in the saturable absorber. The novel nonlinear-effect compensator shows a large nonlinear negative phase-shift depending on input power levels. The proposed concept may open up a novel technology for compensating fiber nonlinearities in optical domain.

5. Slow light optical devices

The manipulation of the speed of light has been attracting much interest in recent years. In particular, slow light appearing in photonic crystals, semiconductor amplifiers, and micro-resonators has been studied for optical buffer memories, optical delay lines, and so on[40−42]. Also, the slow group velocity of light dramatically reduces the size of various optical devices such as optical amplifiers, optical switches, nonlinear optical devices, and so on[43,44]. We have also observed large waveguide dispersion and slow light[45] in Bragg waveguides where light is confined with highly reflective Bragg reflectors[46]. We proposed a slow light modulator with a Bragg waveguide[47,48]. We expect high speed modulation of such an ultra-compact waveguide modulator, which enables us to avoid velocity-matching traveling-wave schemes. An important issue is the coupling between free-space propagation light and slow light.

The group velocity decreases with increasing the waveguide dispersion when the wavelength approaches to the cut-off wavelength. The slow-down factor, which

is defined as the ratio of the group velocity of slow light versus that in conventional semiconductor waveguides, is over 10 in the wavelength range of 1550 − 1560 nm. Thus, the electro-absorption effect is enhanced by a factor of more than 10 in this wavelength range and we are able to reduce the size. Even for an ultra-compact modulator, we expect an extinction ratio of 7 dB over 1550 nm, which will be large enough for short-reach optical links. We also expect low polarization dependence, which is very difficult for that of photonic crystal slab waveguides.

An important issue is how to couple with slow light in a Bragg waveguide. We proposed a simple and practical method of a tilt-coupling scheme as shown in Fig. 14[48]. The input beam is off from the vertical axis and the tilt angle is typically 30°. We carried out the full-vectorial numerical simulation using the film-mode-matching method (FIMMWAVE, Photon Design Co.). Figure 14 shows the model and the calculated field distribution[48]. The coupling loss is less than 1.5 dB for TE and TM modes with a 4 μm-spot-size Gaussian beam input. This coupling scheme enables us to excite slow light propagating in a Bragg waveguide where light is confined by Bragg mirrors.

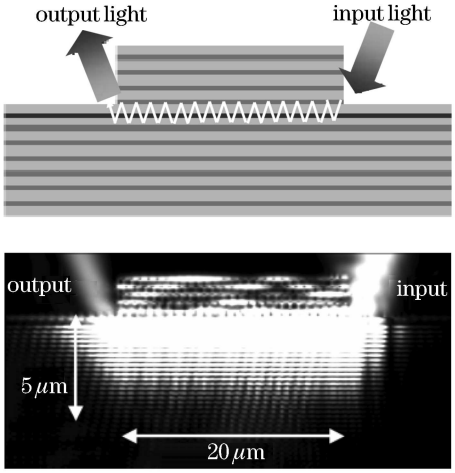

Fig. 14. Calculation model and calculated intensity distribution with tilt light input for efficient excitation of slow light[48].

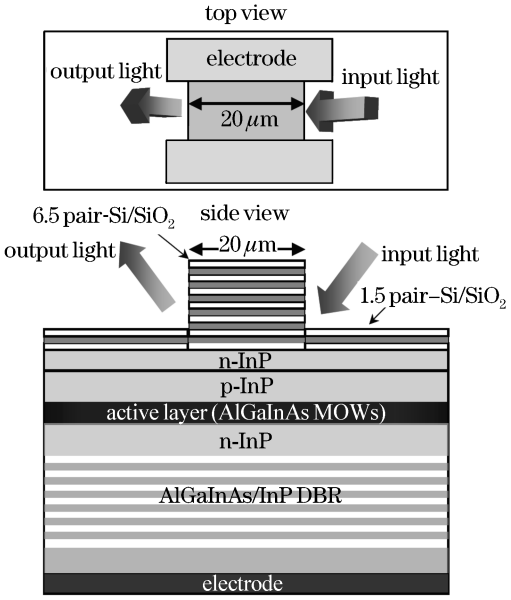

Fig. 15. Schematic structure of a slow light AlGaInAs MQW electro-absorption modulator[48].

We fabricated an electroabsorption modulator consisting of Bragg waveguides with slow light enhancement as shown in Fig. 15[48]. The base structure is similar to that of a conventional InP-based VCSEL without tunnel junction[12]. The bottom mirror is AlGaInAs quarter-wavelength stack mirror. At first, 1.5-pairs Si/SiO_2 dielectric mirror was deposited over the entire surface except top electrodes and then a 5-pair Si/SiO_2 dielectric mirror was partly deposited to form a 20-μm-long Bragg waveguides. The role of 1.5-pair Si/SiO_2 dielectric mirror is the efficient excitation of slow light in a Bragg waveguide. The absorption layer consists of AlGaInAs MQWs in a 1.5-μm wavelength band. With applying reverse bias voltages in its p-n junction, an electro-absorption takes place.

We measured the zero-biased insertion loss from the measured near-field intensity. We could achieve a minimum coupling loss of 1 dB, indicating the low coupling loss of the proposed coupling scheme. We achieved an extinction ratio of 6 dB and an insertion loss of 2 dB for a 20-μm-long compact waveguide modulator. The proposed structure can be monolithically integrated with VCSELs. The proposed modulator would be useful for ultrahigh speed short reach optical links. In addition, simple coupling scheme with slow light in Bragg waveguides would also be useful for slow light photonic circuits involving optical switches, amplifiers, lasers, and so on.

6. Plasmonic VCSELs

High-density optical data storages with Tera-bytes capacity have been attracting much interest. An optical near-field technology is one of candidates to make a breakthrough for future optical storages[49,50]. A storage density of Tera bit/inch^2 is expected when we reduce the spot size to be in the range of 10 nm. A high-density optical disk system using a VCSEL array was proposed[51] and a metal nano-aperture VCSEL was demonstrated for producing optical near-field localized at the metal nano-aperture[52]. The voltage change induced by scattering in a nano-aperture enables us to use the same nano-aperture VCSEL chip for optical near-field probing[52].

A high spatial resolution can be expected by reducing the physical size of the metal aperture. However, the optical near-field intensity through a metal aperture is decreased with decreasing the diameter of the aperture, which is a common difficulty in near-field optics. It is a challenge to enhance the optical near-field from nano-aperture VCSELs. An interesting approach for increasing an optical near-field is to use surface plasmon in metallic nano-structures[53,54]. Surface plasmon excited on a nano particle results in the significant increase of near field intensity.

The schematic structure of a fabricated metal-aperture VCSEL is shown in Fig. 16[52]. The device includes a Au nano-particle in the center of the metal aperture for plasmon enhancement of optical near-fields. The diameter of the metal aperture and a Au particle are 200 nm and 100 nm, respectively. The number of the p-type distributed Bragg reflector (DBR) pair was designed to be about a half of a standard design for increasing the near-field

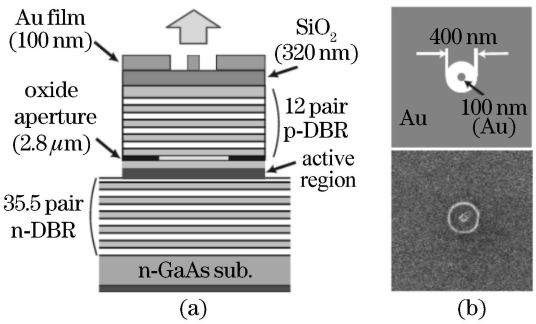

Fig. 16. (a) Schematic structure and (b) top view of a fabricated nano-aperture VCSEL with a Au particle[52].

intensity through the nano-aperture. The structure except the top mirror design and the metal nano-aperture is the same as the conventional GaAs VCSELs. The lasing wavelength was 850 nm. Here, we reduced the diameter of an oxide aperture for increasing the power density in a VCSEL cavity. The diameter of an oxide aperture is as small as 1.7 μm. An small oxide aperture is also helpful for transverse mode control. The threshold is as low as 300 μA.

Optical near-field measurement was carried out. The measurement system is based on a commercially available scanning near-field optical microscopy (SNOM) head (Seiko Instruments Inc.: model SPA300). An aluminum-covered, sharpened fiber probe was scanned in the x, y direction just above the nano-aperture of the fabricated VCSEL. The distance between the fiber probe and the VCSEL was controlled to be constant and to be less than 20 nm by feedback control in the non-contact atomic force microscopy (AFM) mode of SNOM system. When the fiber probe is approaching to the nano-aperture, the scattering from the fiber probe results in threshold changes of the VCSEL. This causes the change in a diode voltage under operating at a constant current. The spatial resolution of the SNOM is 130 nm. This setup also enables us to measure the topography of the device surface at the same time.

Figures 17(a) and (b) show the measured optical near-field intensity and voltage change of the nano-aperture VCSEL with a Au nano-particle, respectively[52]. The spot size of optical near-field measured by SNOM shown in Fig. 17 is estimated to be 100 nm. The power density of optical near-field localized at the nano-aperture is as large as 0.84 MW/cm^2, which is almost 10 times larger than that of conventional VCSELs, which results from strong optical confinement in the oxide micro-cavity and plasmon enhancement. The maximum power density is currently limited by thermal roll-over and the appearance of high-order transverse modes. The proposed near-field

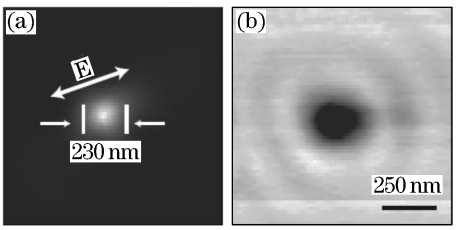

Fig. 17. (a) Measured near-fied intensity and (b) voltage signal of 200 nm metal-aperture VCSEL[52].

VCSEL may provide us with ultra-high power density at low power consumption, which may be useful for future optical storages and optical sensing applications. Recent activities on plasmonic VCSELs include various metallic nano-structures for giant enhancement of optical near-fields[55].

7. Conclusion

Some of recent advances on VCSEL photonics were reviewed, including the wavelength engineering and new functions of VCSELs. The small footprint of VCSELs allowed us to form a densely packed VCSEL array both in space and in wavelength. The wavelength engineering of VCSELs may open up ultra-high capacity networking. In addition, new functions of VCSEL structures for optical signal processing were addressed, which include the manipulation of optical phase, slow light optical devices, and plasmonic VCSELs. These new functionalities may give us new opportunities of VCSEL photonics for new era of optoelectronics.

This work was supported by Grant-in-Aid for Creative Scientific Research from the Ministry of Education, Science, Sport and Culture (#14GS0212") and was partly by NICT. Fumio Koyama's e-mail address is koyama@pi.titech.ac.jp.

References

1. K. Iga, IEEE J. Sel. Top. Quantum Electron. **6,** 1201 (2000).
2. N. Nishiyama, M. Arai, S. Shinada, M. Azuchi, T. Miyamoto, F. Koyama, and K. Iga, IEEE J. Sel. Top. Quantum Electron. **7,** 242 (2001).
3. C. Asplund, P. Sundgren, S. Mogg, M. Hammar, U. Christiansson, V. Oscarsson, C. Runnström, E. Ödling, and J. Malmquist, Electron. Lett. **38,** 635 (2002).
4. T. Kondo, M. Arai, T. Miyamoto, and F. Koyama, *LEOS 2003, Tucson, USA* WD2 (2003).
5. J. A. Lott, N. N. Ledentsov, V. M. Ustinov, N. A. Maleev, A. E. Zhukov, A. R. Kovsh, M. V. Maximov, B. V. Volovik, Zh. I. Alferov, and D. Bimberg, Electron. Lett. **36,** 1384 (2000).
6. T. Anan, M. Yamada, K. Nishi, K. Kurihara, K. Tokutome, A. Kamei, and S. Sugou, Electron. Lett. **37,** 566 (2001).
7. K. D. Choquette, J. F. Klem, A. J. Fischer, O. Blum, A. A. Allerman, I. J. Fritz, S. R. Kurtz, W. G. Breiland, R. Sieg, K. M. Geib, J. W. Scott, and R. L. Naone, Electron. Lett. **36,** 1388 (2000).
8. B. Borchert, A. Y. Egorov, S. Illek, M. Komainda, and H. Riechert, Electron. Lett. **35,** 2204 (1999).
9. T. Kageyama, T. Miyamoto, S. Makino, N. Nishiyama, F. Koyama, and K. Iga, IEEE Photon. Technol. Lett. **12,** 10 (2000).
10. J. Jewell, L. Graham, M. Crom, K. Maranowski, J. Smith, and T. Fanning, Proc. SPIE **6132,** 613204 (2006).
11. M. Ortsiefer, S. Baydar, K. Windhorn, E. RonnCeberg, J. Rosskopf, R. Shau, M. Grau, G. M. Bohm, and M.-C Amann, IEEE Photon. Technol. Lett. **17,** 1596 (2005).
12. N. Nishiyama, C. Caneau, B. Hall, G. Guryanov, M. Hu, X. Liu, M. J. Li, R. Bhat, and C.-E. Zah, IEEE J. Sel. Top. Quantum Electron. **11,** 990 (2005).
13. C. J. Chang-Hasnain, IEEE J. Sel. Top. Quantum Electron. **6,** 978 (2000).

14. M. Huang, Y. Zhou, and C. J. Chang-Hasnain, Nature Photon. **2,** 180 (2008).
15. F. Koyama and K. Iga, *Quantum Optoelectronics of 1997 OSA Spring Topical Meeting* 9, 90 (1997).
16. W. Janto, K. Hasebe, N. Nishiyama, C. Caneau, T. Sakaguchi, A. Matsutani, P. Babu Dayal, F. Koyama, and C.E. Zah, *IEEE International Semiconductor Laser Conference* PD1.1, Hawaii (2006).
17. S. Suda, F. Koyama, N. Nishiyama, C. Caneau, and C. E. Zah, *Conference on Lasers and Electro-Optics 2006* paper CWK3 (2006).
18. C. J. Chang-Hasnain, J. P. Harbison, C. E. Zah, M. W. Maeda, L. T. Florez, N. G. Stoffel, and T. P. Lee, IEEE J. Quantum Electron. **27,** 1368 (1991).
19. F. Koyama, T. Mukaihara, Y. Hayashi, N. Ohnoki, N. Hatori, and K. Iga, IEEE Photon. Technol. Lett. **7,** 10 (1995).
20. L. E. Eng, K. Bacher, Y. Wupen, J. S. Harris, Jr., and C. J. Chang-Hasnain, IEEE J. Sel. Top. Quantum Electron. **1,** 624 (1995).
21. G. G. Oritz, S. Q. Luong, S. Z. Sun, J. Cheng, H. Q. Hou, G. A. Vawer, and B. E. Hammons, IEEE Photon. Technol. Lett. **9,** 1069 (1997).
22. K. Yang, Y. Zhou, X. D. Huang, C. P. Hains, and J. Cheng, IEEE Photon. Technol. Lett. **10,** 377 (2000).
23. D. Schlenker, T. Miyamoto, Z. Chen, F. Koyama, and K. Iga, IEEE Photon. Technol. Lett. **11,** 946 (1999).
24. F. Koyama, D. Schlenker, T. Miyamoto, Z. Chen, A. Matsutani, T. Sakaguchi, and K. Iga, Electron. Lett. **35,** 1079 (1999).
25. T. Kondo, M. Arai, T. Miyamoto, and F. Koyama, Electron. Lett. **40,** 65 (2004).
26. N. Nishiyam, C. Caneau, S. Tsuda, G. Guryanov, M. Hu, R. Bhat, and Chung-En Zah, IEEE Photon. Technol. Lett. **17,** 1605 (2005).
27. M. Arai, T. Kondo, A. Onumura, A. Matsutani, T. Miyamoto, and F. Koyama, IEEE J. Sel. Top. Quantum Electron. **9,** 1367 (2003).
28. Y. Uchiyama, T. Kondo, K. Takeda, A. Matsutani, T. Uchida, T. Miyamoto, and F. Koyama, Jpn. J. Appl. Phys. **44,** L214 (2005).
29. N. Kitabayashi, A. Matsutani, and F. Koyama, International Symposium Contemporary Photon. Technol. **7,** 79 (2007).
30. T. Amano, F. Koyama, M. Arai, and A. Matsutani, Jpn. J. Appl. Phys. **42,** L1377 (2003).
31. C. H. Chang, L. Chrostowski, and C. J. Chang-Hasnain, IEEE J. Quantum Electron. **9,** 1386 (2003).
32. J. Y. Law, G. H. M. van Tartwijk, and G. P. Agrawal, Quantum Semiclass. Opt. **9,** 737 (1997).
33. Y. Hong, P. S. Spencer, P. Rees, and K. A. Shore, IEEE J. Quantum Electron. **38,** 274 (2002).
34. A. Valle, L. Pesquera, S. I. Turovets. and J. M. López, Opt. Commun. **208,** 173 (2002).
35. H. Kawaguchi, Y. Yamayoshi, and K. Tamura, *CLEO 2000* CWU2, 379 (2000).
36. Y. Onishi, N. Nishiyama, C. Caneau, F. Koyama, and C.-E. Zah, IEEE Photon. Technol. Lett. **16,** 1236 (2004).
37. K. Hasebe, F. Koyama, N. Nishiyama, C. Caneau, and C. E. Zah, *Conference on Lasers and Electro-Optics 2006* paper CWP1 (2006).
38. S. Suda, F. Koyama, N. Nishiyama, C. Caneau, and C. E. Zah, *ECOC 2006* Th1.4.7 (2006).
39. S. Suda, F. Koyama, N. Nishiyama, C. Caneau, and C. E. Zah, *IEEE ISLC 2008* TuC1, Sorrento (2008).
40. M. Notomi, K. Yamada, A. Shinya, J. Takahashi, C. Takahashi, and I. Yokohama, Phys. Rev. Lett. **87,** 235902 (2001).
41. A. Yariv, Y. Xu, R. K. Lee, and A. Scherer, Opt. Lett. **24,** 711713 (1999).
42. X. Zhao, P. Palinginis, B. Pesala, C. J. Chang-Hasnain, and P. Hemmer, *ECOC 2005* postdeadline paper, Th4.3.6 (2005).
43. M. Soljacic, S. G. Johnson, S. Fan, M. Ibanescu, E. Ippen, and J. D. Joannopoulas, J. Opt. Soc. Am. B **19,** 2052 (2002).
44. E. Mizuta, H. Watanabe, and T. Baba, Jpn. J. Appl. Phys. **45,** 6116 (2006).
45. Y. Sakurai and F. Koyama, Jpn. J. Appl. Phys. **43,** 5828 (2004).
46. P. Yeh and A. Yariv, J. Opt. Soc. Am **68,** 1196 (1978).
47. K. Kuroki and F. Koyama, *12th Microoptics Conference, (MOC), Seoul, (Korea)* J-1, 222 (2006).
48. G. Hirano, F. Koyama, K. Hasebe, T. Sakaguchi, N. Nishiyama, C. Caneau, and Chung-En Zah, *OFC 2007* Post-deadline paper, PDP34, Anaheim (2007).
49. M. Ohtsu, *Near-Field Nano/Atom Optics and Technology* (Springer-Verlag, Tokyo, 1998).
50. A. Partovi, D. Peale, M. Wuttig, C. A. Murray, G. Zydzik, L. Hopkins, K. Baldwin, W. S. Hobson, J. Wynn, J. Lopata, L. Dhar, R. Chichester, and J. H.-J. Yeh, Appl. Phys. Lett. **75,** 1515 (1999).
51. K. Goto, Jpn. J. Appl. Phys. **37,** 2274 (1998).
52. J. Hashizume and F. Koyama, Opt. Express **12,** 6391 (2004).
53. T. Thio, H. F. Ghaemi, H. J. Lezec, P. A. Wolff, and T. W. Ebbesen, J. Opt. Soc. Am. B **16,** 1743 (1999).
54. T. Thio, K. M. Pellerin, R. A. Linke, H. J. Lezec, and T. W. Ebbesen, Opt. Lett. **26,** 1972 (2001).
55. Z. Rao, L. Hesselink, and J. S. Harris, Opt. Lett. **32,** 1995 (2007).